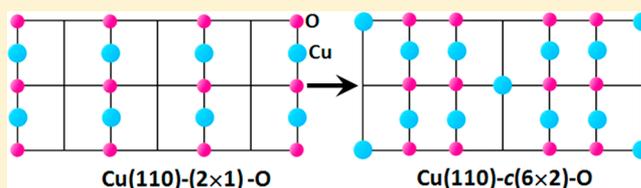# Kinetic Barriers of the Phase Transition in the Oxygen Chemisorbed Cu(110)-(2 × 1)-O as a Function of Oxygen Coverage

Liang Li,[†] Qianqian Liu,[†] Jonathan Li,[‡] Wissam A. Saidi,[§] and Guangwen Zhou*,[†]

[†]Department of Mechanical Engineering & Multidisciplinary Program in Materials Science and Engineering and [‡]Department of Physics, Applied Physics and Astronomy & Multidisciplinary Program in Materials Science and Engineering, State University of New York, Binghamton, New York 13902, United States

[§]Department of Mechanical Engineering and Materials Science, University of Pittsburgh, Pittsburgh, Pennsylvania 15261, United States

ABSTRACT: Oxygen chemisorption induced surface reconstructions are widely observed, but the atomic processes leading to transitions among oxygen chemisorbed phases are largely unknown. Using ab initio molecular dynamics and density-functional theory, we study the kinetic process of the Cu(110)-(2 × 1) → $c(6 × 2)$ phase transition upon increasing oxygen surface coverage. We show that the phase transition

involves initially Cu−O dimer and Cu−O−Cu trimer formation with a kinetic barrier of ∼0.13 eV, followed by a barrierless process of forming a four Cu−O−Cu−O chains configuration that transitions to the $c(6 × 2)$ reconstruction via concerted movement of three Cu atoms with an associated energy barrier of ∼1.41 eV. The larger kinetic barrier is suggested as the origin of the kinetic hindrance that is inferred from the significant discrepancy between the experimentally observed temperature and pressure dependent (2 × 1) → $c(6 × 2)$ phase transition and the equilibrium thermodynamics prediction.

I. INTRODUCTION

Oxygen chemisorbed layers on metal surfaces display frequently rather complex structures resulting from interactions of adsorbed oxygen atoms not just with the substrate but with each other as well. Such interactions are of particular importance in many crucial technological processes such as oxidation, corrosion, and heterogeneous catalysis as well as in fundamental studies of two-dimensional phase transitions. Although considerable works studying oxygen chemisorption exists both experimentally and theoretically, the understanding of adatom−adatom interactions is still quite limited. The study of oxygen chemisorption induced phase transformation in an oxygen chemisorbed layer upon increasing oxygen surface coverage promises to be an important approach in obtaining a quantitative understanding of the interactions that adatoms undergo.

In particular, the oxidation of copper surfaces has been investigated extensively due to its critical role in a variety of practical fields, including electronic device fabrication and chemical catalysis.[1−3] Among the low index copper surfaces, the O/Cu(110) system is especially interesting because oxygen chemisorption on Cu(110) induces two distinct reconstructions preceding the formation of bulk oxide. At the oxygen coverage of 0.5 monolayer (ML), the Cu(110) surface reconstructs to a (2 × 1) phase, which is characterized by the formation of Cu−O−Cu chains growing preferentially along the [001] direction in every other [1̄10]-(1 × 1) spacing.[4−12] Upon increasing oxygen surface coverage, the (2 × 1) reconstruction transits to a $c(6 × 2)$ reconstruction with a saturated oxygen coverage $\theta = 2/3$,[13,14] which contains two

adjacent [001]-oriented Cu−O−Cu chains in every three [1̄10]-(1 × 1) lattice spacings. These structures have been supported by different experiments using a variety of experimental tools.[15−21] However, despite receiving considerable attention, an atomic level understanding of the (2 × 1) → $c(6 × 2)$ transition at finite temperature and pressure still remains elusive.

The reconstruction of a metal surface implies not only a morphological change but generally also remarkable change in chemical reactivity. For instance, it was found that the reaction of methanol on clean Cu(110) and oxygen precovered Cu(110) is very sensitive to preadsorbed oxygen induced reconstruction.[22−24] This suggests that the identification of the surface structure under real conditions is a basic step to obtain insight into the O/Cu(110) system. Recently, using scanning tunneling microscopy (STM), we monitored the sequential formation of the (2 × 1) and $c(6 × 2)$ reconstructions under controlled oxygen pressure and temperature. By comparing with the theoretical phase diagram obtained from ab initio thermodynamics, we found that the oxygen pressure leading to the (2 × 1) → $c(6 × 2)$ transition observed in experiments is 10 orders of magnitude higher than the theoretical prediction.[25] Such a significant difference is attributed to the effect of kinetic hindrance that prevents the surface from establishing equilibrium with the imposed oxygen chemical potential. In fact, the significant discrepancy between equilibrium phase
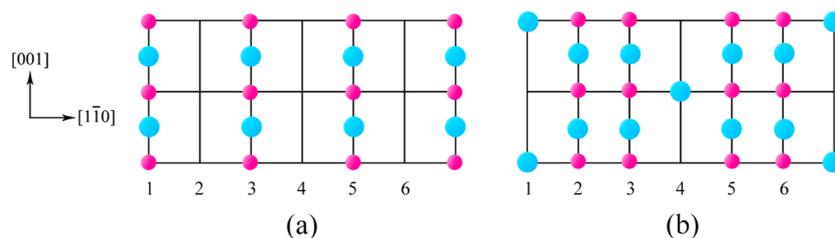
Figure 1. Schematic illustrations of the top layer of (a) Cu(110)-(2 × 1) and (b) Cu(110)-c(6 × 2) surface phase, where Cu atoms are depicted by blue balls and oxygen atoms by red balls.

diagram predictions and experimental realities was also observed on Cu (100),[26] and also similar kinetic hindrance effects were observed for other metallic systems.[27−32] For instance, Lundgren et al. performed an *in situ* study on the oxidation of Pd(100) surface at oxygen pressures in the range of 10^{-6}–10^3 mbar using surface X-ray diffraction and noted the strong kinetic hindrance to bulk oxide formation from an oxygen chemisorbed phase even at a temperature as high as 675 K.[33]

The atomic mechanism for the origin of such kinetic hindrance is not established because the real-time atomic evolution during the surface phase transition is unknown. The lack of this knowledge is due largely to the inability of experimental approaches with sufficient detectability to resolve the dynamic process of the surface phase transition at the atomic scale. Identification of the cause of the kinetic hindrance for surface oxidation is important not only for properly understanding the experimental observations but also for manipulating the oxidation of metals. Fortunately, atomistic theoretical approaches can provide an effective tool to investigate the nature of the dynamic transition of the atomic structures despite the small time scales of the reactions. In this work, we employ density-functional theory (DFT) as well as ab initio molecular dynamics (AIMD) techniques to study the energetics and kinetics of the Cu(110)-(2 × 1) → c(6 × 2) transition upon increasing oxygen surface coverage. AIMD has proved effective and accurate in studying early stage oxidation of metal surfaces and the properties in metal–oxygen systems.[34−38] Our study aims to identify potential reaction pathways and the associated energy barriers for the formation of the c(6 × 2) structure from the oxygen chemisorbed (2 × 1) phase. The validity of the assumptions made in the simulations is checked by experimental scanning tunneling microscopy (STM) imaging of the oxygen chemisorbed Cu(110) surface. By elucidating these atomic steps and energy barriers, our results provide an atomistic picture for understanding the origin of kinetic hindrance in the oxygen chemisorption induced surface phase transition as well as the insight into the details of Cu and O adatom interaction in the chemisorbed layer.

II. COMPUTATIONAL METHODS AND EXPERIMENTAL DETAILS

DFT calculations are performed using the generalized gradient approximation (GGA) of Perdew−Wang (PW91)[39] for the exchange-correlation functional, as implemented in the Vienna Ab-initio Simulation Package (VASP).[40−43] We use projector augmented wave (PAW)[44,45] potentials in conjunction with a plane-wave cutoff energy of 380 eV. All of the simulation cells in this study have the same size, so the Brillouin-zone integration is performed using (2 × 4 × 1) Monkhorst−Pack grids[46] for all the cells. The calculations are carried out with

broadening of the Fermi surface according to Methfessel−Paxton smearing technique[47] with a smearing parameter of 0.2 eV. All of our calculations are spin-averaged except for those involving free molecular and atomic oxygen where the calculations are spin polarized. The Cu surfaces are modeled using a periodically repeated slab with five layers where the bottom layer is fixed. The image slabs along the direction perpendicular to the surface are separated by a vacuum region of 11 Å. The positions of all the atoms, except those of the bottom layer, are allowed to relax fully in all three dimensions until the force components acting on each atom are less than 0.015 eV/Å. Our calculated lattice constant for Cu is 3.64 Å using a Monkhorst−Pack grid of (11 × 11 × 11), which is in good agreement with the experimental value 3.61 Å[48] and with previous calculations.[49−51]

We applied the climbing image nudged elastic bands (CI-NEB) method[52] to calculate the reaction barriers, where at least five intermediate images are added in between the initial and final states. The adsorption energy of oxygen is calculated as

$$E_O^{ads} = \frac{1}{N_O}\left(E_{O/Cu}^{tot} - E_{ref} + \frac{N_O}{2}E_{O_2}\right)$$

where $E_{O/Cu}^{tot}$ is the total energy of the Cu−O system and E_{ref} is the energy of the structure before adsorbing oxygen. E_{O_2} is the energy of an isolated oxygen molecule, and N_O is the number of oxygen adatoms added into the system, which is equal to 1 in this work as one oxygen adatom is added at a time. We performed various tests to validate the computational framework such as **k**-grid convergence, plane-wave cutoff, and vacuum size and found that the values adopted in this work yield sufficiently converged energies. For example, the changes in the oxygen adsorption energy on a clean (2 × 1) surface using a **k**-grid of (4 × 8 × 1), a plane-wave cutoff energy of 450 eV, and a vacuum size of 15 Å are within 0.04, 0.02, and 0.01 eV of the values obtained using the lower thresholds, respectively. In particular, this shows that the vacuum size is sufficiently large, and there is no need to apply the dipole correction.

All AIMD calculations are performed starting from the relaxed structures obtained by DFT calculations, with no initial velocities assigned. The simulations are carried out in a canonical ensemble (NVT) with a Nosé thermostat[53] for temperature control. The systems are first heated up through velocity scaling to 500 K (some calculations are repeated using 700 K, and essentially the same results are obtained) with a heating rate of about 500 K/ps and subsequently annealed at the same temperature for at least 7 ps for further equilibration. The time step for constant temperature MD simulation is chosen to be 2 fs, which is sufficient to yield reliable morphological and energetic properties. The time step adopted in this paper is smaller than those used in some other AIMD works on metal−oxygen systems.[37,38,54]
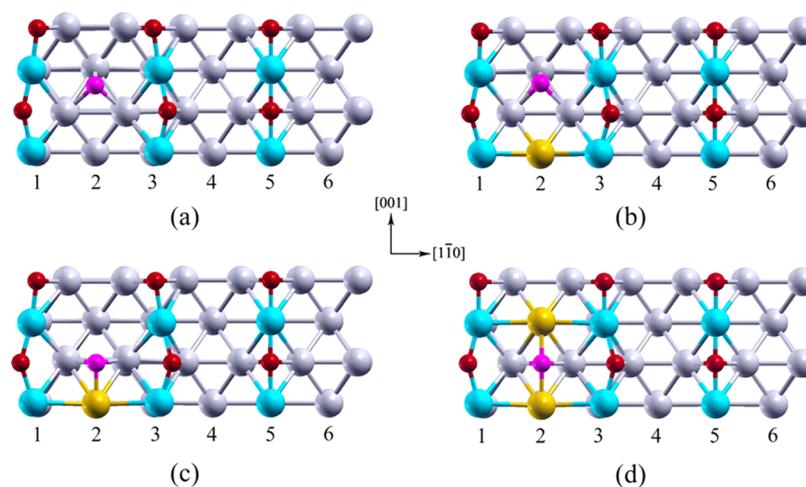
Figure 2. Fully relaxed structures when Cu and O adatoms are added consecutively into the (2×1) phase. (a) One O adatom is added into row 2. (b) One Cu adatom is added into row 2. (c) The O and Cu adatoms introduced in (a) and (b) form a Cu−O dimer. (d) A second Cu adatom is added into the system and form a trimer structure together with the previously adsorbed adatoms. For better illustration, the top-layer Cu and O atoms of the original (2×1) phase are depicted by blue and red balls, respectively, and the substrate Cu atoms by gray balls. Cu and O adatoms are depicted by yellow and purple balls, respectively.

To validate some of the results in our simulations, a variable-temperature ultrahigh vacuum scanning tunneling microscope (Omicron VT-AFM XA) was employed to image the atomic structures of oxygen chemisorbed Cu(110) surfaces. The Cu(110) single crystal used in the STM experiment is a "top-hat" disk, purchased from Princeton Scientific Corp., cut to within 0.1° to the (110) crystallographic orientation and polished to a mirror finish. The crystal was cleaned by repeated cycles of Ar⁺ sputtering and annealing. A variable-pressure leak valve was used for controlled oxygen dosing. STM imaging was performed at room temperature in constant-current mode with bias on the sample.

III. RESULTS

A. Overview. The structural difference between the (2×1) and $c(6 \times 2)$ reconstructions lies in the configuration of the topmost atomic layer. Figure 1 shows the structural models of the top layer of the oxygen chemisorbed Cu(110)-(2×1) and $c(6 \times 2)$ phases, in which the same cell sizes are used for the two oxygen chemisorbed phases. The simulation cell for the (2×1) top layer has six Cu atoms and six O atoms with an oxygen coverage of 0.5 ML, while the cell for the $c(6 \times 2)$ top layer contains ten Cu atoms and eight O atoms with an oxygen surface coverage of 2/3 ML. This suggests that the Cu(110)-$(2 \times 1) \rightarrow c(6 \times 2)$ transition requires incorporation of additional Cu and O atoms; i.e., four extra Cu atoms and two extra O atoms are required to add into the existing (2×1) phase to reach the same surface coverage of Cu and O atoms in the $c(6 \times 2)$ phase. Meanwhile, the $(2 \times 1) \rightarrow c(6 \times 2)$ transition requires breaking up the added Cu−O−Cu rows in the (2×1) reconstruction in order to accommodate additional Cu and O atoms. The breakdown of the Cu−O−Cu chain was assumed initially to require a large kinetic barrier, due to the prevailing belief that there are strong bonds acting on the surface Cu and O atoms, which effectively stabilize the whole system.[55−57] However, as presented later in this paper, our study shows that the Cu−O bond breaking can also be a barrierless process.

The direct experimental evidence about the dynamic picture of the phase transition is still unreachable due to the lack of experimental tools with sufficient detectability in resolving the atomic processes, and thus the reaction pathways derived from simulation results seem to be unjustified. However, taking into account the dependence of phase transition on the adatom incorporation, this work does not completely rely on intuitive deductions. To get a good insight, we first carry out AIMD calculations by adding Cu and O atoms into the (2×1) structure and letting the system evolve and equilibrate and then obtain the ground state geometries and energies by DFT relaxations. Once a feasible path of the $(2 \times 1) \rightarrow c(6 \times 2)$ phase transition is obtained from AIMD, we then utilize NEB calculations to quantitatively determine the kinetics associated with the transition. Such an interplay between AIMD and NEB can minimize the bias due to an arbitrary starting guess, yielding a more accurate representation of phase transitions.

B. AIMD and DFT Calculations. We first have a close look at the structural difference of the (2×1) and $c(6 \times 2)$ phases. While Cu−O−Cu chains serve as building blocks for both structures, $c(6 \times 2)$ clearly has a higher density of Cu−O−Cu chains. The assembly of more chains in the (2×1) structure requires breaking up the native Cu−O−Cu chains and deposition of additional Cu and O atoms. Noticing that both the (2×1) and $c(6 \times 2)$ structures have Cu−O−Cu chains in row 3 and row 5 (shown in Figure 1), it would be sensible to keep the Cu−O−Cu chains in row 3 and row 5 intact when simulating the phase transition, in order to minimize the mass transport and bond breaking. Therefore, a natural choice is to assemble new chains in row 2 and row 6 via the supply of extra Cu and O atoms.

Starting with the perfect (2×1) phase shown in Figure 1a, we first place an O atom on row 2 in a prerelaxed (2×1) surface with an arbitrary distance of approximately 3.0 Å above the surface,[36,37] so that the system can freely evolve starting from 0 K. The system is heated up to 500 K through velocity scaling, followed by a 7 ps equilibration period. After equilibration, the O atom is found to adsorb at the shifted-hollow (ShH) site of the second atomic layer, which is consistent with our previous study on the subsurface oxygen adsorption of the $c(6 \times 2)$ surface.[58] The configuration obtained by AIMD is then further relaxed in a subsequent DFT calculation, which gives the final geometry as shown in Figure
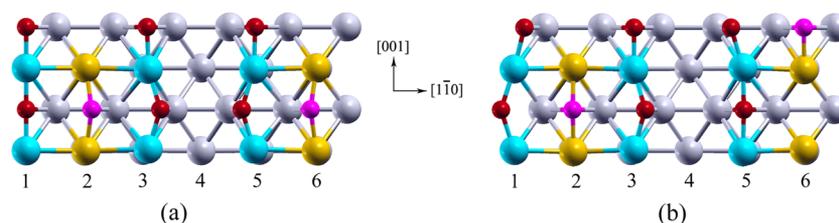
Figure 3. Double-trimer configurations relaxed by DFT calculations. (a) The two trimers are symmetric with respect to row 4. (b) The trimer in row 6 of (a) is displaced by one $[001]$-(1×1) lattice spacing.
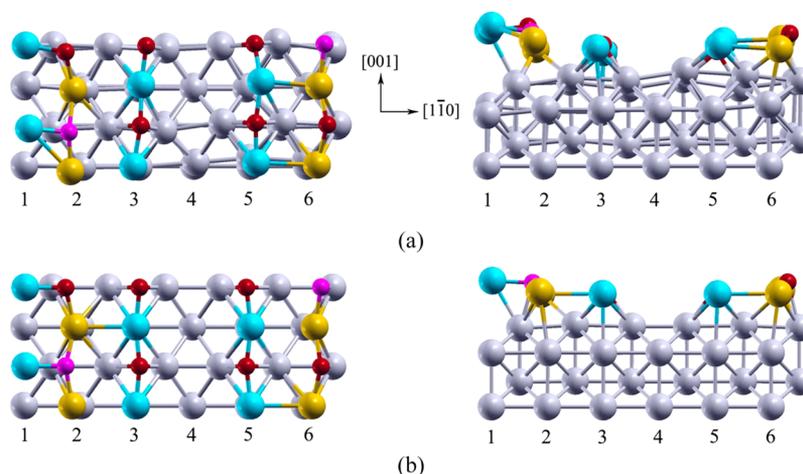

Figure 4. (a) Top (left) and side (right) view of the last snapshot of the AIMD simulation starting from the structure shown in Figure 3b. (b) Top (left) and side (right) view of the structure shown in (a) after geometry relaxation.
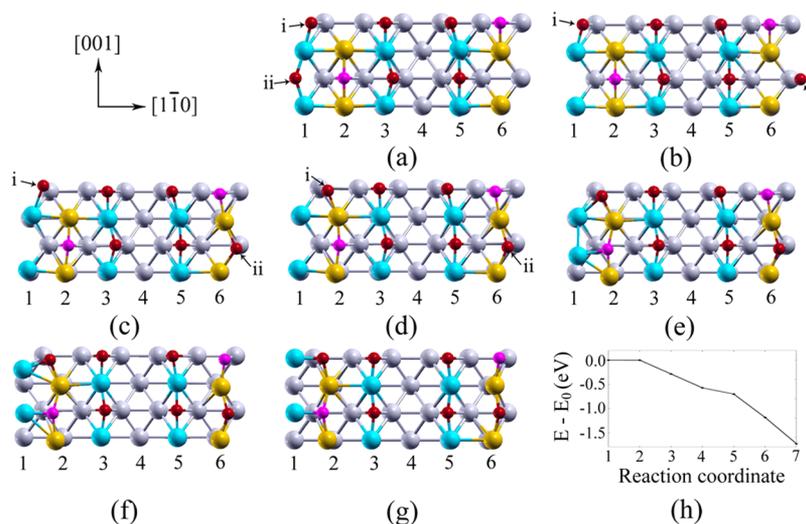

Figure 5. (a) Two-trimer configuration, which is the starting image of the NEB calculation. (b–f) The relaxed intermediate NEB images. (g) Four-chain configuration obtained in the AIMD run, which is also the final image of the NEB calculation. (h) NEB energy plot for the morphology transition.

2a. The adsorption energy of the oxygen atom is calculated to be −1.16 eV. Because the formation of the Cu−O−Cu chain-like structure requires alternate arrangement of O and Cu atoms, we then place a Cu atom in row 2 at the Cu lattice point and obtain the structure shown in Figure 2b. NEB calculation reveals that the reaction barrier to form the Cu−O dimer structure as shown in Figure 2c is as small as 0.13 eV, and this configuration is proved to be stable after 7 ps of AIMD relaxation in the canonical ensemble at 500 K. Meanwhile, the system energy decreases by 0.28 eV due to the dimer

formation. Thus, this step is both kinetically and thermodynamically favorable. By a further relaxation using AIMD started by placing additional Cu atom in row 2, a Cu−O−Cu trimer is naturally formed, as illustrated in Figure 2d.

Now we have the crucial component of a Cu−O−Cu chain in row 2. Considering the symmetry of the $c(6 \times 2)$ structure, we then need to build another Cu−O−Cu trimer in row 6, but an issue arises on the exact location of the second trimer. Since the first trimer is preadsorbed in row 2, there are two possible places for the trimer in row 6. First, as the configuration shown
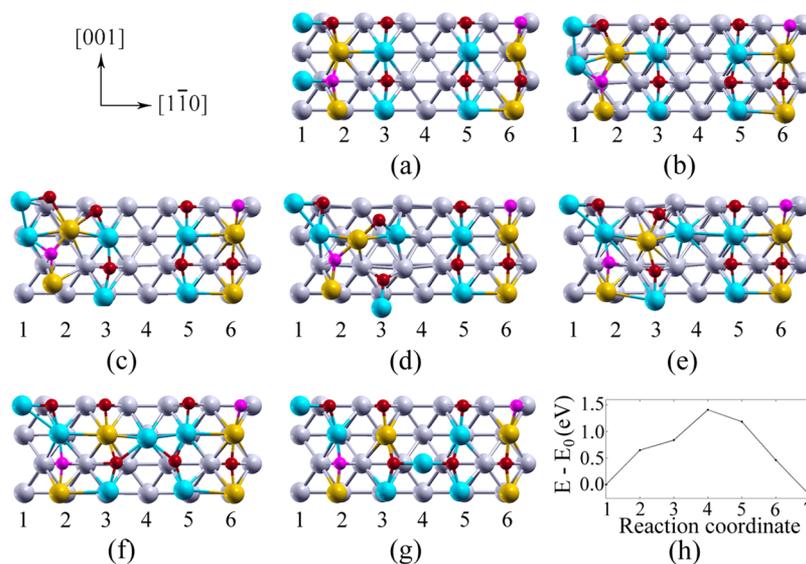
Figure 6. (a) Four-chain configuration, which is the starting image of the NEB calculation. (b−f) The relaxed intermediate NEB images. (g) The Cu(110)-$c(6 \times 2)$ configuration, which is the final image of the NEB calculation. (h) NEB energy plot for the concerted Cu movement.

in Figure 3a, the two trimers in row 2 and row 6 could be symmetric with respect to row 4, and second, as the configuration shown in Figure 3b, the trimer adsorbed in row 6 is displaced by one [001]-(1×1) lattice spacing (i.e., ∼3.64 Å) comparing with that in Figure 3a. Because of the translational symmetry of the unit cell along the [001] direction, the only difference between the two configurations in Figure 3 lies in the positions of the oxygen atoms. Our DFT calculations reveal that the system energy of the configuration in Figure 3b is 0.33 eV more stable than that of Figure 3a. Therefore, we choose the configuration in Figure 3b to be an intermediate state as the (2×1) phase transforms to the $c(6 \times 2)$ phase. Notice that starting from this configuration we have achieved the same coverage of Cu and O as that in the $c(6 \times 2)$ unit cell, which implies that ideally the $c(6 \times 2)$ phase can be achieved by rearrangement of the Cu and O atoms, namely by breaking some of the Cu−O bonds in the configuration shown in Figure 3b. To determine the possible reaction paths for bond breaking and atom arrangement, AIMD calculations are performed starting with the configuration shown in Figure 3b. The system is expected to evolve toward the lowest-energy structure, which is the experimentally observed $c(6 \times 2)$.

By heating the system up to 500 K and then maintaining the system at this temperature for 10 ps in the NVT ensemble, we reach a structure with four rows of Cu−O−Cu chains, as shown in Figure 4a. This four-chain structure obtained by the AIMD treatment is then further relaxed using DFT, which results in an equilibrium structure illustrated in Figure 4b. A close comparison between Figures 4a and 4b reveals that after the DFT structural relaxation the overall geometry of the system does not show pronounced changes, and all the atom positions are altered only marginally, which indicate that the structure obtained by AIMD is fairly close to equilibrium. We then perform NEB calculations to quantitatively study the transition from Figure 3b to Figure 4b. Figures 5a−g display the intermediate snapshots of the transition, which reveal that the transition involves rearrangement of a few atoms. First, as shown in Figures 5a−d, the Cu−O−Cu chain in row 1 is broken and the two O atoms labeled by i and ii are dislodged from row 1. The O atom labeled by i moves to the adjacent

2 and attach with the Cu atom of the existing Cu−O−Cu trimer to form a Cu−O−Cu−O chain along the [001] direction. The O atom labeled by ii moves to the adjacent row 6 and attach to the Cu atom of the existing Cu−O−Cu trimer to form a Cu−O−Cu−O chain along the [001] direction. Second, as shown in Figures 5e−g, the two Cu atoms left behind in row 1 move by 1/2 [001]-(1×1) lattice spacing (i.e., ∼1.8 Å) to bond with the two O atoms in row 2. Figure 5h depicts the energy landscape of the transition from the double-trimer configuration in Figure 3b to the four-chain configuration in Figure 4b, which shows that the system total energy decreases throughout the reaction. Therefore, it is clear that after two Cu−O−Cu trimers are sequentially adsorbed in row 2 and row 6 of the (2×1) structure, the system then spontaneously evolves to the configuration of Figure 4b, resulting in a significant drop of the system total energy by 1.73 eV. It is noted that although the transition from Figure 3b to Figure 4b is initiated by Cu−O bond breaking in row 1, surprisingly there is no reaction barrier associated with this process.

Now the system geometry closely resembles that of the $c(6 \times 2)$ reconstruction. In both structures, there are two Cu−O−Cu−O chains in every three [1̄10]-(1×1) lattice spacings, whereas the differences are in the positions of the two Cu atoms that are not involved in the formation of the Cu−O−Cu−O chains in rows 2 and 6. Figure 6a is the same configuration shown in Figure 5g, and Figure 6g is the configuration of the $c(6 \times 2)$ reconstruction. As seen in Figure 6a, row 1 has two Cu atoms while row 4 is vacant, whereas in the $c(6 \times 2)$ structure (Figure 6g), the two Cu atoms are redistributed with one located in row 1 and the other one in row 4 and coordinated laterally with the O atoms in the adjacent Cu−O−Cu−O chains. To form the $c(6 \times 2)$ structure, a possible path is the direct dislodgement of one of the Cu atoms in row 1 to the vacant row 4, but such a transition pathway is kinetically unfavorable because the Cu atom has to migrate a long distance over row 2 and 3 to reach row 4. Our NEB calculation indicates that the energy barrier for such direct migration is higher than 2.00 eV, and the Cu atom needs to overcome multiple barriers along the pathway involving several
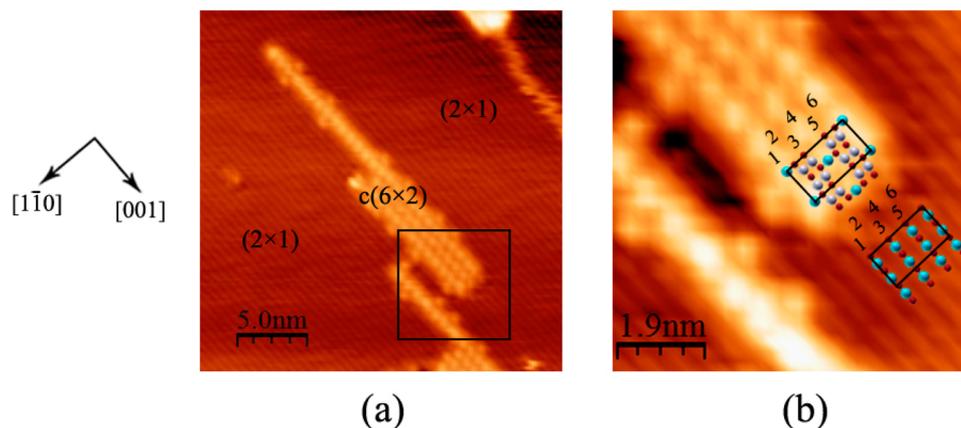
Figure 7. Topographic STM images of Cu(110) oxidized at 150 °C under the oxygen pressure of 10^{-5} Torr for 20 min: (a) the coexistence of the (2×1) and $c(6 \times 2)$ phases; (b) the magnified view of the labeled area in (a), and the ideal positions of Cu and O atoms of the (2×1) phase and $c(6 \times 2)$ phase are represented by blue and red balls, respectively. The Cu atoms of $c(6 \times 2)$ phase that are invisible in the STM observations are indicated by gray balls. The tunneling conditions for the STM imaging are $I_T = 0.1-0.5$ nA and $V_B = -1$ V.

Cu−O bond breakings and bond re-formations. We herein propose an alternative transition path that essentially involves the concerted movement of three Cu atoms by following the pathway as shown in Figures 6a−g. Three Cu atoms from row 1, 2, and 3 move simultaneously, with a lateral displacement of one $[1\bar{1}0]$-(1×1) lattice spacing for each Cu atom, and then end up at the stable locations matching with the $c(6 \times 2)$ structure. The reaction barrier for the concerted movement is 1.41 eV, as seen in Figure 6h. By forming the $c(6 \times 2)$ structure from the configuration shown in Figure 6a, the system total energy decreases marginally by 0.20 eV.

IV. DISCUSSION

The stable structure of an oxygen chemisorbed layer is typically assumed to be in equilibrium with the bulk and oxygen gas, which requires long reaction time to reach. Transitions among surface phases may be limited by various atom transport processes, and thus sometimes the surface phases observed are in some respect metastable because the state of thermodynamic equilibrium is not reached. There are many examples where the thermodynamically stable phase cannot be achieved—either due to kinetic barriers[33,59] or other reasons such as preparation conditions.[60] Sometimes, the discrepancy between a calculated phase stability region and a measured stability region is due to intrinsic errors in the theoretical approach such as in the exchange-correlation functional in DFT calculations or even to the various employed approximations such as neglect of vibrational and entropic contributions. We showed in our previous studies that these errors are unlikely to show substantial changes to the phase diagrams.[25,26]

In our study, the $(2 \times 1) \rightarrow c(6 \times 2)$ phase transition is assumed to occur via the breakup of the existing (2×1) chains followed by the formation of new Cu−O chains, as illustrated in Figure 1. Indeed such a relationship between the atomic arrangements of the (2×1) and $c(6 \times 2)$ phases is observed in our STM experiments. Figure 7 shows representative STM images of a Cu(110) surface exposed to oxygen gas at the pressure = 1×10^{-5} Torr and $T = 150$ °C for 20 min. The topographic image in Figure 7a shows an area of the oxygen chemisorbed Cu(110) surface, on which the$(2 \times 1) \rightarrow c(6 \times 2)$ transition is captured. Figure 7a shows clearly that Cu−O−Cu chains in the two reconstructions are parallel along the $[001]$ direction, consistent with our phase transition model assuming

the formation of new Cu−O−Cu chains in between the existing Cu−O−Cu chains of the (2×1) reconstruction. We particularly examine the boundary area of the two reconstructions, which would give insight into how Cu−O−Cu chains in the (2×1) are converted into $c(6 \times 2)$. Figure 7b shows a zoomed-in view of the boundary area of the two reconstructions and the atomic configuration at their boundary, where the ideal positions of the Cu and O atoms are indicated by blue and red balls, respectively. It should be noted that STM can detect the Cu atoms that are at a higher surface level of the $c(6 \times 2)$ phase (corresponding to the Cu atoms shown in row 1 and row 4 in Figure 1b), which result in the bright spots in Figures 7a and 7b. The rest of the Cu atoms that are not detectable are indicated by gray balls. For comparison, the cells with the same size (i.e., (6×2)) are indicated both on (2×1) and $c(6 \times 2)$ regions. It can be seen that rows 2, 4, and 6 of the originally empty troughs between Cu−O−Cu rows of the (2×1) reconstructed phase are filled up with either Cu−O chains or Cu atoms after the phase transition. The Cu−O−Cu chain in row 1 in the (2×1) phase is broken into discretely distributed Cu atoms after the phase transition. This confirms the proposed mechanism that the phase transition is accompanied by the breakup of some of the native (2×1) chains while adding up new chains in the originally empty $[001]$ troughs.

In our model we provide one possible pathway for the formation of the trimers in row 2 and row 6. It is worth noting that there can be other potential pathways that are unexplored here. For instance, the trimer formation is modeled in Figure 2 by sequentially adding O and Cu adatoms into row 2, but it is also possible that the O and Cu adatoms have already bonded together as Cu−O dimers or even Cu−O−Cu trimers at other places and diffuse across the surface before they are adsorbed into row 2. However, it should be noted that the different possible pathways of forming the Cu−O−Cu trimers do not change our conclusions. This is because the most important aspect in the $(2 \times 1) \rightarrow c(6 \times 2)$ transition is the structural evolution after the formation of the two trimers as the system naturally evolves to the configuration shown in Figure 4b without experiencing energy barriers. Considering the translational symmetry of the system, the configuration shown in Figure 3b can be identically visualized as that shown in Figure 8, in which the continuous chain structure in row 1 is perceived as two segments adjacent to row 2 and row 6, respectively. Such
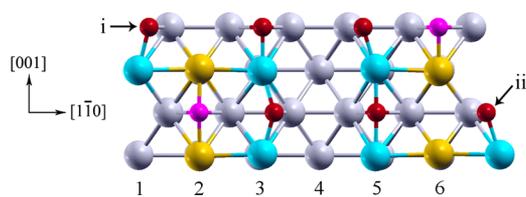
Figure 8. An alternative visualization of the double-trimer configuration, in which the chain structure in row 1 is split into two segments.

a barrierless transition may be related to the undercoordinated Cu atoms in the Cu−O−Cu trimers in row 2 and row 6, which exert significant attraction force on the O atoms in row 1. By looking at Figure 8, we can clearly observe a strong tendency for O atoms labeled i and ii to move toward row 2 and row 6, respectively. After the transition, the Cu−O bonds in row 1 are broken, and meanwhile new bonds are formed in row 2 and row 6. The two Cu atoms left behind in row 1 also shift by 1/2 [001]-(1 × 1) lattice spacing to coordinate laterally with the O atoms in the adjacent rows. Therefore, the overall number of Cu−O bonds has increased, which results in the decrease in the system total energy.

The last step of the transition leading to the formation of the $c(6 \times 2)$ structure is the concerted movement of the three Cu atoms shown in Figure 6. This is the only transition step that is not observed in our AIMD simulations, which maybe partly attributed to the fact that the time scale of the AIMD run is not sufficient to see such a subtle reaction. The energy barrier for the concerted movement is calculated as 1.41 eV, which is the largest barrier among all the atomic processes involved in the (2 × 1) → $c(6 \times 2)$ transition. The experimentally observed kinetic hindrance for the (2 × 1) → $c(6 \times 2)$ most likely originates from this step of the concerted movement of three Cu atoms.

As a matter of fact, we have annealed the structure shown in Figure 4b at 1000 K for 10 ps, and no structural changes are observed. In the AIMD simulation, the concerted movement of Cu atoms does not occur even at such a high temperature, but in the experiments, the phase transition has been observed at much lower temperatures.[25] The reason is that in the NEB calculations the effect of temperature is precluded. In reality, the reaction barrier is lower than that calculated by NEB because of the temperature contribution. Therefore, the calculated value of 1.41 eV is the theoretical upper bound of this phase transition barrier.

It is worthwhile mentioning that the potential reaction pathway of the phase transitions is not unique. To confirm that the pathway described in this work is indeed feasible, i.e., the associated energy barrier is low enough compared with other paths, we have also explored other possible reaction mechanisms. For instance, we have tested the reaction by depositing a Cu adatom in row 4 of the clean (2 × 1) phase (Figure 1a) followed by adding Cu and O adatoms in row 2 and row 6, respectively, no morphology change toward the $c(6 \times 2)$ phase is observed in the subsequent AIMD simulations, and the barriers for atom rearrangements are large.

The formation of the (2 × 1) reconstruction was shown to occur by an added-row process via surface diffusion of Cu atoms detached from surface steps or terraces and O atoms supplied from dissociative oxygen chemisorption on a non-reconstructed or reconstructed Cu(110) surface.[7,8] The energy barrier for the dissociation of oxygen molecules on a nonreconstructed Cu(110) surface is 0 eV along the [001] direction and 0.12 eV along the [1$\bar{1}$0] direction.[61−63] Upon increasing oxygen coverage, the Cu(110) surface undergoes (2 × 1) reconstruction first and then $c(6 \times 2)$ formation prior to the bulk oxide formation. For the dissociation of molecular O$_2$ on the (2 × 1) reconstruction, our DFT calculations show that the most favorable site for the adsorption of an oxygen molecule is the hollow (H) site of the second Cu layer in between two existing Cu−O−Cu−O chains, and our NEB calculations indicate that the dissociation of oxygen molecules occurs spontaneously with no energy barrier along the [001] direction, while if the oxygen molecule is adsorbed along the [1$\bar{1}$0] direction at the H site of the reconstructed surface, the molecule decomposes to two separate atoms in the DFT relaxed structure, indicating that [1$\bar{1}$0] is not a favorable adsorption orientation for molecular oxygen. The supply of extra oxygen also involves surface diffusion of atomic oxygen on a nonreconstructed or the (2 × 1) reconstructed Cu(110) surfaces for the (2 × 1) → $c(6 \times 2)$ phase transition. Using NEB, we find that the barriers for O diffusion on a nonreconstructed Cu(110) surface along the [1$\bar{1}$0] and [001] directions are 0.21 and 0.30 eV, respectively, and the barrier for the diffusion of atomic oxygen on (2 × 1) chemisorbed layer along the [100] direction in between the Cu−O−Cu−O chains is 0.53 eV. The diffusion along [1$\bar{1}$0] direction of (2 × 1) chemisorbed layer is unlikely because adatoms need to jump over the Cu−O−Cu−O chains.

Regarding the addition of extra Cu adatoms into the chemisorbed system, the main source of Cu adatoms are surface defects (e.g., via step-edge detachment) for the initial stages of the phase transition. Our NEB calculations indicate that the energy barrier for Cu detachment from a single-atomic height step is 0.53 eV. The supply of additional Cu adatoms from terraces is also possible if the supply of Cu adatoms from step edges does not keep up with impinging oxygen flux.[25] We have thus calculated the energy barriers for Cu removal from a nonreconstructed Cu(110) terrace and a (2 × 1) reconstructed Cu(110) terrace, which are found to have the values of 0.72 and 0.82 eV, respectively. Similarly, the (2 × 1) →$c(6 \times 2)$ phase transition also involves surface diffusion of Cu adatoms on a nonreconstructed or the (2 × 1) reconstructed Cu(110) surfaces. Our calculations show that the energy barriers for Cu diffusion in the [1$\bar{1}$0] and [001] directions of the non-reconstructed Cu(110) are 0.29 and 0.31 eV, respectively, and the energy barrier for Cu diffusion on the (2 × 1) reconstructed surface along the [100] direction in between two Cu−O−Cu−O chains is 1.15 eV. The values of our calculated diffusion barriers for Cu and O adatoms on the nonreconstructed Cu(110) surface are also consistent with previous studies.[51]

Compared to all these atomic processes for the (2 × 1) reconstruction, the energy barrier (1.41 eV) for the concerted movement of the Cu atoms involved in the (2 × 1) → $c(6 \times 2)$ transition is still the largest throughout the two sequential reconstructions. The kinetic barrier of 1.41 eV associated with the concerted movement of Cu atoms in the $c(6 \times 2)$ reconstruction formation corroborates with an earlier *in situ* electron microscopy study that monitored the nucleation events of Cu$_2$O islands on Cu(110), from which the activation energy for Cu$_2$O nucleation was determined to be 1.1 ± 0.2 eV.[64] This agreement suggest that the energy barrier for oxygen subsurface diffusion for nucleating Cu$_2$O may be comparable to or smaller than the energy barrier for the concerted movement of Cu atoms in the $c(6 \times 2)$ reconstruction. This is likely by

considering the fact that the structure for the $c(6 \times 2)$ reconstruction is still pretty open with vacant sites in rows 1 and 4 (see Figure 1b), which may facilitate oxygen subsurface adsorption without experiencing significantly energy barrier.

V. SUMMARY

In this work, we use both AIMD and NEB techniques to investigate the kinetic process of the $(2 \times 1) \rightarrow c(6 \times 2)$ phase transition upon increasing oxygen coverage on Cu(110). Our results indicate that the formation of Cu−O dimers and Cu−O−Cu trimers during the initial steps of the surface phase transition requires only small kinetic barriers, which is followed by a barrierless process of transforming to a configuration containing four Cu−O−Cu−O chains. Although the four-chain configuration resembles the $c(6 \times 2)$ reconstruction, its transition to the $c(6 \times 2)$ structure requires the concerted movement of three Cu atoms with an associated energy barrier of 1.41 eV, which is the largest barrier throughout the $(2 \times 1) \rightarrow c(6 \times 2)$ transition. This barrier is suggested to be the origin of the kinetic hindrance that causes discrepancy between the experimentally observed temperature and pressure dependent $(2 \times 1) \rightarrow c(6 \times 2)$ and the theoretical O/Cu(110) equilibrium phase diagram obtained by the first-principles thermodynamics. We expect that the approach proposed in this study may be applicable to study the microscopic processes of other oxygen chemisorption induced surface phase transitions.

■ AUTHOR INFORMATION

Corresponding Author

*E-mail gzhou@binghamton.edu (G.Z.).

Notes

The authors declare no competing financial interest.

■ ACKNOWLEDGMENTS

■ REFERENCES

(1) Huang, T.; Tsai, D. CO Oxidation Behavior of Copper and Copper Oxides. *Catal. Lett.* **2003**, *87*, 173−178.

(2) White, B.; Yin, M.; Hall, A.; Le, D.; Stolbov, S.; Rahman, T.; Turro, N.; O'Brien, S. Complete CO Oxidation over Cu₂O Nanoparticles Supported on Silica Gel. *Nano Lett.* **2006**, *6*, 2095−2098.

(3) Jing, F.; Zhang, Y.; Luo, S.; Chu, W.; Zhang, H.; Shi, X. Catalytic Synthesis of 2-Methylpyrazine over Cr-Promoted Copper Based Catalyst via a Cyclo-Dehydrogenation Reaction Route. *J. Chem. Sci.* **2010**, *122*, 621−630.

(4) Ertl, G. Untersuchung von Oberflächenreaktionen Mittels Beugung Langsamer Elektronen (LEED): I. Wechselwirkung von O2 Und N2O Mit (110)-, (111)- Und (100)-Kupfer-Oberflächen. *Surf. Sci.* **1967**, *6*, 208−232.

(5) DiDio, R. A.; Zehner, D. M.; Plummer, E. W. An Angle-Resolved UPS Study of the Oxygen-Induced Reconstruction of Cu(110). *J. Vac. Sci. Technol., A* **1984**, *2*, 852−855.

(6) Jacobsen, K. W.; Nørskov, J. K. Theory of the Oxygen-Induced Restructuring of Cu(110) and Cu(100) Surfaces. *Phys. Rev. Lett.* **1990**, *65*, 1788−1791.

(7) Coulman, D. J.; Wintterlin, J.; Behm, R. J.; Ertl, G. Novel Mechanism for the Formation of Chemisorption Phases: The (2×1) O-Cu (110) "Added-Row" Reconstruction. *Phys. Rev. Lett.* **1990**, *64*, 1761−1764.

(8) Jensen, F.; Besenbacher, F.; Lægsgaard, E.; Stensgaard, I. Surface Reconstruction of Cu(110) Induced by Oxygen Chemisorption. *Phys. Rev. B* **1990**, *41*, 10233−10236.

(9) Ruan, L.; Besenbacher, F.; Stensgaard, I.; Laegsgaard, E. Atom Resolved Discrimination of Chemically Different Elements on Metal Surfaces. *Phys. Rev. Lett.* **1993**, *70*, 4079−4082.

(10) Uehara, Y.; Matsumoto, T.; Ushioda, S. Identification of O Atoms on a Cu(110) Surface by Scanning Tunneling Microscope Light Emission Spectra. *Phys. Rev. B* **2002**, *66*, 075413.

(11) Bobrov, K.; Guillemot, L. Interplay between Adsorbate-Induced Reconstruction and Local Strain: Formation of Phases on the Cu(110)-(2 × 1):O Surface. *Phys. Rev. B* **2008**, *78*, 121408.

(12) Duan, X.; Warschkow, O.; Soon, A.; Delley, B.; Stampfl, C. Density Functional Study of Oxygen on Cu(100) and Cu(110) Surfaces. *Phys. Rev. B* **2010**, *81*, 075430.

(13) Feidenhans'l, R.; Grey, F.; Nielsen, M.; Besenbacher, F.; Jensen, F.; Laegsgaard, E.; Stensgaard, I.; Jacobsen, K. W.; Nørskov, J. K.; Johnson, R. L. Oxygen Chemisorption on Cu (110): A Model for the c(6 × 2) Structure. *Phys. Rev. Lett.* **1990**, *65*, 2027−2030.

(14) Feidenhans'l, R.; Grey, F.; Johnson, R. L.; Nielsen, M. Determination of the Cu (110)-c(6× 2)-O Structure by X-Ray Diffraction. *Phys. Rev. B* **1991**, *44*, 1875−1879.

(15) Bronckers, R. P. N.; de Wit, A. G. J. Reconstruction of the Oxygen-Covered Cu{110} Surface Identified with Low Energy Ne⁺ and H₂O⁺ Ion Scattering. *Surf. Sci.* **1981**, *112*, 133−152.

(16) Döbler, U.; Baberschke, K.; Haase, J.; Puschmann, A. Azimuthal- and Polar-Angle-Dependent Surface Extended X-Ray—Absorption Fine-Structure Study: (2 × 1)O on Cu(110). *Phys. Rev. Lett.* **1984**, *52*, 1437−1440.

(17) Niehus, H.; Comsa, G. Determination of Surface Reconstruction with Impact-Collision Alkali Ion Scattering. *Surf. Sci.* **1984**, *140*, 18−30.

(18) Parkin, S. R.; Zeng, H. C.; Zhou, M. Y.; Mitchell, K. A. R. Low-Energy Electron-Diffraction Crystallographic Determination for the Cu(110)2 × 1-O Surface Structure. *Phys. Rev. B* **1990**, *41*, 5432−5435.

(19) Moritz, W.; Zuschke, R.; Pflanz, S.; Wever, J.; Wolf, D. Adsorption Induced Reconstruction of the Cu(110) Surface. *Surf. Sci.* **1992**, *272*, 94−101.

(20) Dorenbos, G.; Breeman, M.; Boerma, D. O. Low-Energy Ion-Scattering Study of the Oxygen-Induced Reconstructed p(2 × 1) and c(6 × 2) Surfaces of Cu(110). *Phys. Rev. B* **1993**, *47*, 1580−1588.

(21) Dürr, H.; Fauster, T.; Schneider, R. Surface Structure Determination of the (2×1)O-Cu(110) Reconstruction by Low-Energy Ion Scattering. *Surf. Sci.* **1991**, *244*, 237−246.

(22) Silva, S. L.; Lemor, R. M.; Leibsle, F. M. STM Studies of Methanol Oxidation to Formate on Cu(110) Surfaces: I. Sequential Dosing Experiments. *Surf. Sci.* **1999**, *421*, 135−145.

(23) Demirci, E.; Stettner, J.; Kratzer, M.; Schennach, R.; Winkler, A. Methanol Adsorption on Cu(110) and the Angular Distribution of the Reaction Products. *J. Chem. Phys.* **2007**, *126*, 164710.

(24) Singnurkar, P.; Bako, I.; Koch, H. P.; Demirci, E.; Winkler, A.; Schennach, R. DFT and RAIRS Investigations of Methanol on Cu(110) and on Oxygen-Modified Cu(110). *J. Phys. Chem. C* **2008**, *112*, 14034−14040.

(25) Liu, Q.; Li, L.; Cai, N.; Saidi, W. A.; Zhou, G. Oxygen Chemisorption-Induced Surface Phase Transitions on Cu(110). *Surf. Sci.* **2014**, *627*, 75−84.

(26) Saidi, W. A.; Lee, M.; Li, L.; Zhou, G.; McGaughey, A. J. H. Ab Initio Atomistic Thermodynamics Study of the Early Stages of Cu (100) Oxidation. *Phys. Rev. B* **2012**, *86*, 245429.

(27) Li, W.-X.; Stampfl, C.; Scheffler, M. Insights into the Function of Silver as an Oxidation Catalyst by Ab Initio Atomistic Thermodynamics. *Phys. Rev. B* **2003**, *68*, 165412.

(28) Reuter, K.; Stampfl, C.; Ganduglia-Pirovano, M. V.; Scheffler, M. Atomistic Description of Oxide Formation on Metal Surfaces: The Example of Ruthenium. *Chem. Phys. Lett.* **2002**, *352*, 311−317.

(29) Klikovits, J.; Napetschnig, E.; Schmid, M.; Seriani, N.; Dubay, O.; Kresse, G.; Varga, P. Surface Oxides on Pd(111): STM and Density Functional Calculations. *Phys. Rev. B* **2007**, *76*, 045405.

(30) Vlad, A.; Stierle, A.; Marsman, M.; Kresse, G.; Costina, I.; Dosch, H.; Schmid, M.; Varga, P. Metastable Surface Oxide on CoGa(100): Structure and Stability. *Phys. Rev. B* **2010**, *81*, 115402.

(31) Westerström, R.; Weststrate, C.; Gustafson, J.; Mikkelsen, A.; Schnadt, J.; Andersen, J.; Seriani, N.; Mittendorfer, F.; Kresse, G.; et al. Lack of Surface Oxide Layers and Facile Bulk Oxide Formation on Pd(110). *Phys. Rev. B* **2009**, *80*, 125431.

(32) Westerström, R.; Weststrate, C. J.; Resta, A.; Mikkelsen, A.; Schnadt, J.; Andersen, J. N.; Lundgren, E.; Schmid, M.; Seriani, N.; Harl, J.; et al. Stressing Pd Atoms: Initial Oxidation of the Pd(110) Surface. *Surf. Sci.* **2008**, *602*, 2440−2447.

(33) Lundgren, E.; Gustafson, J.; Mikkelsen, A.; Andersen, J. N.; Stierle, A.; Dosch, H.; Todorova, M.; Rogal, J.; Reuter, K.; Scheffler, M. Kinetic Hindrance during the Initial Oxidation of Pd(100) at Ambient Pressures. *Phys. Rev. Lett.* **2004**, *92*, 046101.

(34) Colombi Ciacchi, L.; Payne, M. C. "Hot-Atom" O_2 Dissociation and Oxide Nucleation on Al(111). *Phys. Rev. Lett.* **2004**, *92*, 176104.

(35) Colombi Ciacchi, L.; Payne, M. C. First-Principles Molecular-Dynamics Study of Native Oxide Growth on Si(001). *Phys. Rev. Lett.* **2005**, *95*, 196101.

(36) Zimmermann, J.; Finnis, M. W.; Colombi Ciacchi, L. Vacancy Segregation in the Initial Oxidation Stages of the TiN(100) Surface. *J. Chem. Phys.* **2009**, *130*, 134714.

(37) Zimmermann, J.; Colombi Ciacchi, L. Mechanisms of Initial Oxidation of the Co(0001) and Cr(110) Surfaces. *J. Phys. Chem. C* **2010**, *114*, 6614−6623.

(38) Fang, H. Z.; Wang, W. Y.; Jablonski, P. D.; Liu, Z. K. Effects of Reactive Elements on the Structure and Diffusivity of Liquid Chromia: An Ab Initio Molecular Dynamics Study. *Phys. Rev. B* **2012**, *85*, 014207.

(39) Perdew, J. P.; Chevary, J. A.; Vosko, S. H.; Jackson, K. A.; Pederson, M. R.; Singh, D. J.; Fiolhais, C. Atoms, Molecules, Solids, and Surfaces: Applications of the Generalized Gradient Approximation for Exchange and Correlation. *Phys. Rev. B* **1992**, *46*, 6671−6687.

(40) Kresse, G.; Hafner, J. Ab Initio Molecular Dynamics for Liquid Metals. *Phys. Rev. B* **1993**, *47*, 558−561.

(41) Kresse, G.; Hafner, J. Ab Initio Molecular-Dynamics Simulation of the Liquid-Metal−Amorphous-Semiconductor Transition in Germanium. *Phys. Rev. B* **1994**, *49*, 14251−14269.

(42) Kresse, G.; Furthmüller, J. Efficiency of Ab-Initio Total Energy Calculations for Metals and Semiconductors Using a Plane-Wave Basis Set. *Comput. Mater. Sci.* **1996**, *6*, 15−50.

(43) Kresse, G.; Furthmüller, J. Efficient Iterative Schemes for Ab Initio Total-Energy Calculations Using a Plane-Wave Basis Set. *Phys. Rev. B* **1996**, *54*, 11169−11186.

(44) Blöchl, P. E. Projector Augmented-Wave Method. *Phys. Rev. B* **1994**, *50*, 17953−17979.

(45) Kresse, G.; Joubert, D. From Ultrasoft Pseudopotentials to the Projector Augmented-Wave Method. *Phys. Rev. B* **1999**, *59*, 1758−1775.

(46) Monkhorst, H. J.; Pack, J. D. Special Points for Brillouin-Zone Integrations. *Phys. Rev. B* **1976**, *13*, 5188−5192.

(47) Methfessel, M.; Paxton, A. High-Precision Sampling for Brillouin-Zone Integration in Metals. *Phys. Rev. B* **1989**, *40*, 3616−3621.

(48) Ashcroft, N. W.; Mermin, N. D. *Solid State Physics*; Saunders College: Rochester, NY, 1976.

(49) Kangas, T.; Laasonen, K.; Puisto, A.; Pitkänen, H.; Alatalo, M. On-Surface and Sub-Surface Oxygen on Ideal and Reconstructed Cu(100). *Surf. Sci.* **2005**, *584*, 62−69.

(50) Alatalo, M.; Jaatinen, S.; Salo, P.; Laasonen, K. Oxygen Adsorption on Cu(100): First-Principles Pseudopotential Calculations. *Phys. Rev. B* **2004**, *70*, 245417.

(51) Liem, S. Y.; Kresse, G.; Clarke, J. H. R. First Principles Calculation of Oxygen Adsorption and Reconstruction of Cu(110) Surface. *Surf. Sci.* **1998**, *415*, 194−211.

(52) Henkelman, G.; Uberuaga, B. P.; Jónsson, H. A Climbing Image Nudged Elastic Band Method for Finding Saddle Points and Minimum Energy Paths. *J. Chem. Phys.* **2000**, *113*, 9901−9904.

(53) Nosé, S. A Molecular Dynamics Method for Simulations in the Canonical Ensemble. *Mol. Phys.* **1984**, *52*, 255−268.

(54) Belonoshko, A. B.; Ahuja, R.; Eriksson, O.; Johansson, B. Quasi-Ab Initio Molecular Dynamic Study of Cu Melting. *Phys. Rev. B* **2000**, *84*, 3838−3844.

(55) Besenbacher, F.; Norskov, F. B. Oxygen Chemisorption on Metal Surfaces: General Trends for Cu, Ni and Ag. *Prog. Surf. Sci.* **1993**, *44*, 5−66.

(56) Jaatinen, S.; Blomqvist, J.; Salo, P.; Puisto, A.; Alatalo, M.; Hirsimäki, M.; Ahonen, M.; Valden, M. Adsorption and Diffusion Dynamics of Atomic and Molecular Oxygen on Reconstructed Cu(100). *Phys. Rev. B* **2007**, *75*, 075402.

(57) Piccinin, S.; Stampfl, C.; Scheffler, M. Ag−Cu Alloy Surfaces in an Oxidizing Environment: A First-Principles Study. *Surf. Sci.* **2009**, *603*, 1467−1475.

(58) Li, L.; Zhou, G. W. Oxygen Subsurface Adsorption on the Cu(110)-c(6 × 2) Surface. *Surf. Sci.* **2013**, *615*, 57−64.

(59) Reuter, K.; Scheffler, M. Composition and Structure of the RuO2(110) Surface in an O_2 and CO Environment: Implications for the Catalytic Formation of CO_2. *Phys. Rev. B* **2003**, *68*, 045407.

(60) Reuter, K.; Scheffler, M. Composition, Structure, and Stability of $RuO_2(110)$ as a Function of Oxygen Pressure. *Phys. Rev. B* **2001**, *65*, 035406.

(61) Ge, J.-Y.; Dai, J.; Zhang, J. Z. H. Dissociative Adsorption of O_2 on Cu(110) and Cu(100): Three-Dimensional Quantum Dynamics Studies. *J. Phys. Chem.* **1996**, *100*, 11432−11437.

(62) Liem, S. Y.; Clarke, J. H. R.; Kresse, G. Pathways to Dissociation of O_2 on Cu (110) Surface: First Principles Simulations. *Surf. Sci.* **2000**, *459*, 104−114.

(63) Sun, L. D.; Hohage, M.; Zeppenfeld, P. Oxygen-Induced Reconstructions of Cu(110) Studied by Reflectance Difference Spectroscopy. *Phys. Rev. B* **2004**, *69*, 045407.

(64) Zhou, G. W.; Yang, J. C. Initial Oxidation Kinetics of Copper (110) Film Investigated by in Situ UHV-TEM. *Surf. Sci.* **2003**, *531*, 359−367.